Amino Acid Complexes of Metal Carbonyls: Mechanistic Aspects of the CO-Labilizing Ability of Glycinate Ligands in Zero-Valent Chromium and Tungsten Derivatives†

Donald J. Darensbourg,* Jennifer D. Draper, and Joseph H. Reibenspies

Department of Chemistry, Texas A&M University, College Station, Texas 77843

Received November 6, 1996⊗

The amino and phosphino acid derivatives of chromium(0) and tungsten(0), $[Et_4N][Cr(CO)_4(O_2CCH_2NH_2)]$ (**1**), $[Et_4N][Cr(CO)_4(O_2CCH_2NHMe)]$ (**2**), $[Et_4N][Cr(CO)_4(O_2CCH_2NMe_2)]$ (**3**), $[Et_4N][W(CO)_4(O_2CCH(C(CH_3)_3)NH_2)]$ (**4**), $[Et_4N][W(CO)_4(O_2CCH(C_6H_5)NH_2)]$, $[Et_4N][W(CO)_4(O_2CCH_2PPh_2)]$ (**5**), and $[Et_4N][Cr(CO)_4(O_2CCH_2PPh_2)]$ have been synthesized from the reaction of the $M(CO)_5THF$ adduct with the tetraethylammonium salt of the corresponding amino or phosphino acid in THF solution. The complexes have been characterized in solution by ^{13}C NMR and infrared spectroscopies and in the solid state by X-ray crystallography. The geometry of the metal anion is, in each case, that of a distorted octahedron consisting of four carbonyl ligands and a puckered five-membered glycinate chelate ring, bound through the nitrogen atom and one of its oxygen atoms. Notable about complex **1** is that the crystal obtained exhibited both a different morphology and a different space group than its tungsten analogue. Examination of the packing diagram reveals that this change is due to the different orientation of the chelate ring in **1** relative to the corresponding orientation in the $W(CO)_4(O_2CCH_2NH_2)^-$ anion. Complexes **1** and **2** exhibit intermolecular hydrogen-bonding interactions between the amine N−H group and the distal oxygen on an adjacent molecule, with N···O distances of 2.828 and 2.821 Å, respectively. Investigations of the lability of the carbonyl ligands have been carried out. The lability is proposed to be due to base-assisted removal of a proton from the amine ligand leading to a substitutionally labile amide transient species. The tungsten analogue of complex **1** was used to obtain evidence in support of this mechanism. The isotope effect (k_H/k_D) was measured for $W(CO)_4(O_2CCH_2NH_2)^-$ using d_5-glycine and was found to be 2.34. The activation parameters for the intermolecular exchange of CO in the $[Et_4N][W(CO)_4(O_2CCH_2NH_2)]$ salt were determined and found to be $\Delta H^{\ddagger} = 15.4 \pm 1.0$ kcal/mol and $\Delta S^{\ddagger} = -23.2 \pm 3.2$ eu, values consistent with the proposed mechanism. In addition, the effect of substitution of electron-donating ($C(CH_3)_3$) and electron-withdrawing (C_6H_5) substituents on the methylene carbon was evaluated. There was little change in the rate of CO exchange observed for $W(CO)_4(O_2CCH(C(CH_3)_3)NH_2)^-$ (**5**) and $W(CO)_4(O_2CCH(C_6H_5)NH_2)^-$ *vs* $W(CO)_4(O_2CCH_2NH_2)^-$, showing that steric or electronic effects away from the N center are not responsible for the observed CO lability. As anticipated on the basis of the proposed substitutional pathway, the phosphino acid metal carbonyl derivatives did not exhibit facile intermolecular CO exchange.

Introduction

Our initial interest in amino acid complexes of zero-valent group-six transition metals was motivated by a desire to mechanistically understand metal-catalyzed decarboxylation processes.[1] These derivatives were of particular concern since we had previously demonstrated that interaction of the carboxylate ligand, *via* an appended distal group, with the metal's center enhances the rate of decarboxylation relative to the free base, e.g., $(CO)_5WNCCH_2CO_2^-$ decarboxylates more rapidly than $[NCCH_2CO_2^-]$.[2] In addition to this matter an issue of importance to our comprehensive efforts in carbon dioxide chemistry involves the structural and reactivity investigation of coordinatively unsaturated metal carbonyl derivatives which are stabilized by π-donation from aryloxide and amide ligands. For example, the series of tungsten tricarbonyl derivatives depicted below have been fully structurally characterized in solution and in the solid state.[3] The amido ligand is thus a good π-donation ligand and is anticipated to be an excellent CO-labilizing group, even better than alkoxides or aryloxides.[4]

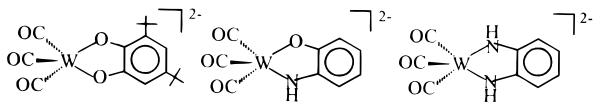

While amino acid derivatives of tungsten carbonyl were being investigated, it was observed that, in those instances where the nitrogen atom contained at least one hydrogen, the CO ligands underwent a facile exchange process with ^{13}CO in solution.[5] That is, the anions $W(CO)_4(O_2CCH_2NH_2)^-$ and $W(CO)_4(O_2CCH_2NHMe)^-$ are subject to the reaction defined in eq 1, whereas the *N,N*-dimethylglycinate complex was inert toward

† Dedicated to Professor R. G. Wilkins on the occasion of his 70th birthday.

⊗ Abstract published in *Advance ACS Abstracts,* July 15, 1997.

(1) Darensbourg, D. J.; Holtcamp, M. W.; Longridge, E. M.; Khandelwal, B.; Klausmeyer, K. K.; Reibenspies, J .H. *J. Am. Chem. Soc.* **1995**, *117*, 318. (b) Darensbourg, D. J.; Holtcamp, M. W.; Khandelwal, B.; Klausmeyer, K. K.; Reibenspies, J. H. *Inorg. Chem.* **1995**, *34*, 2389.

(2) Darensbourg, D. J.; Chojnacki, J. A.; Atnip, E. V. *J. Am. Chem. Soc.* **1993**, *115*, 4675.

(3) (a) Darensbourg, D. J.; Klausmeyer, K. K.; Mueller, B. C.; Reibenspies, J. H. *Angew. Chem., Int. Ed. Engl*. **1992**, *31*, 1503. (b) Darensbourg, D. J.; Klausmeyer, K. K.; Reibenspies, J. H. *Inorg. Chem*. **1996**, *35*, 1529. (c) Darensbourg, D. J.; Klausmeyer, K. K.; Reibenspies, J. H. *Inorg. Chem.* **1996**, *35*, 1535.

(4) (a) Brown, T. L.; Atwood, J. D. *J. Am. Chem. Soc.* **1976**, *98*, 3160. (b) Lichtenberger, D. L.; Brown, T. L. *J. Am. Chem. Soc*. **1978**, *100*, 366. (c) Poulton, J. T.; Flting, K.; Streib, W. E.; Caulton, K. G. *Inorg. Chem.* **1992**, *31*, 3190. (d) Caulton, K. G. *New J. Chem.* **1994**, *18*, 25. (e) Poulton, J. T.; Sigalas, M. P.; Folting, K.; Streib, W. E.; Eisenstein, O.; Caulton, K. G. *Inorg. Chem.* **1994**, *33*, 1476.

(5) Darensbourg, D. J.; Atnip, E. V.; Klausmeyer, K. K.; Reibenspies, J. H. *Inorg. Chem.***1994**, *33*, 5230.

S0020-1669(96)01344-4 CCC: $14.00

CO dissociation under the same reaction conditions. Since the former complexes were shown to hydrogen bond both in solution and in the solid state *via* the N−H moiety, this CO labile was suggested to originate from the intermediary of a transient amido species, much like that proposed in the base-assisted hydrolysis of metal ammine and amine complexes (eq 2).[6]

$$W(CO)_4(O_2CCH_2NHR)^- + {}^{13}CO \underset{R = H, Me}{\rightleftharpoons} W({}^{13}CO)_4(O_2CCH_2NHR)^- + {}^{12}CO \quad (1)$$

$$Co(NH_3)_5X^{2+} + OH^- \rightarrow Co(NH_3)_5OH^{2+} + X^- \quad (2)$$

At this time we wish to compare and contrast the structural and reactivity studies of amino acid derivatives of chromium and tungsten tetracarbonyl. In particular, kinetic evidence will be presented which will serve to better define the mechanistic aspects associated with the enhanced CO lability observed in selected amino acid derivatives. The CO labilities in the metal (diphenylphosphino)acetate tetracarbonyl anions were determined in order to distinguish between electronic effects arising from the carboxylate *vs* amino functionalities.

Experimental Section

Methods and Materials. All manipulations were performed on a double-manifold Schlenk vacuum line under an atmosphere of argon or in an argon-filled glovebox. Solvents were dried and deoxygenated by distillation from the appropriate reagent under a nitrogen atmosphere. Photolysis experiments were performed using a mercury arc 450-W UV immersion lamp purchased from Ace Glass Co. Infrared spectra were recorded on a Mattson 6022 spectrometer with DTGS and MCT detectors. Routine infrared spectra were collected using a 0.10-mm CaF_2 cell. ^{13}C NMR spectra were obtained on a Varian XL-200 spectrometer. ^{13}CO was purchased from Cambridge Isotopes and used as received. $Cr(CO)_6$ and $W(CO)_6$ were purchased from Strem Chemicals, Inc., and used without further purification. Glycine and sarcosine were purchased from Fischer Scientific Company and Aldrich Chemical Company, Inc., respectively, and were washed with THF prior to use. Dimethylglycine (purchased from Aldrich Chemical Company) and deuterated glycine-d_5 (purchased from Cambridge Isotopes) were used without further purification. L-*tert*-Leucine was donated by NSC Technologies and was used as received. 2-Phenylglycine was obtained from Aldrich Chemical Company and used without further purification. (Diphenylphosphino)acetic acid was prepared by the literature method cited.[7] Microanalyses were performed by Galbraith Laboratories, Inc., Knoxville, TN, and Canadian Microanalytical Service, Ltd., Delta, BC, Canada.

Synthesis of $[Et_4N][O_2CCHXNRR']$ and $[Et_4N][O_2CCH_2P(C_6H_5)_2]$ Salts. The synthesis of these salts was accomplished by the addition of 1 equiv (1.4 mmol) of Et_4NOH, 25% in methanol, to the corresponding amino or phosphino acid (where R = H or Me, R′ = H or Me, and X = H, C_6H_5, or $C(CH_3)_3$). The mixture was stirred for 60 min, and the methanol was removed under vacuum overnight, leaving a clear gel (when X = H) or white powder (when X = C_6H_5 or $C(CH_3)_3$).

Synthesis of $[Et_4N][M(CO)_4(O_2CCHXNRR')]$ Derivatives. The synthesis of $[Et_4N][M(CO)_4(O_2CCHXNRR')]$ (where M = W or Cr) was accomplished in yields in excess of 80% by the reaction of 1 equiv of $M(CO)_5THF$ (prepared by the photolysis of 0.300 g of $Cr(CO)_6$ or 0.500 g of $W(CO)_6$ in THF) with 1 equiv (1.4 mmol) of the deprotonated amino acid. THF was removed from the reaction mixture by vacuum, and the resulting light orange solid was washed several times in hexanes to yield a yellow to orange powder. Crystals were grown by the slow diffusion of hexane into a concentrated THF solution of the complex at −10 °C. The extreme air sensitivity of the chromium compounds rendered an accurate analysis, of powder or crystals, difficult to obtain. Nevertheless, the complexes were shown by IR and NMR to be analytically pure. Anal. Calcd for $[Et_4N][Cr(CO)_4(O_2CCH_2NH_2)]$ (**1**) ($C_{14}H_{24}N_2O_6Cr$): C, 45.66; H, 6.57; N, 7.61; O, 26.07. Found: C, 41.61; H, 7.88; N, 7.98; O, 23.78. Anal. Calcd for $[Et_4N][Cr(CO)_4(O_2CCH_2NHMe)]$ (**2**) ($C_{15}H_{26}N_2O_6Cr$): C, 47.13; H, 6.86; N, 7.33; O, 25.11. Found: C, 45.52; H, 7.46; N, 7.58; O, 23.40. Anal. Calcd for $[Et_4N][Cr(CO)_4(O_2CCH_2NMe_2)]$(**3**)($C_{16}H_{28}N_2O_6Cr$): C, 48.49; H, 7.12; N, 7.07; O, 24.22. Found: C, 42.96; H, 7.73; N, 7.37; O, 23.78. Anal. Calcd for $[Et_4N][W(CO)_4(O_2CCH(C(CH_3)_3)NH_2)]$ (**4***)* ($C_{18}H_{32}N_2O_6W$): C, 38.86; H, 5.80; N, 5.04. Found: C, 37.65; H, 5.81; N, 5.04.

Synthesis of $[Et_4N][M(CO)_4(PPh_2CH_2CO_2)]$ Derivatives. The synthesis of $[Et_4N][M(CO)_4(PPh_2CH_2CO_2)]$ (where M = W or Cr) was accomplished in yields in excess of 90% in a manner analogous to that described for the amino acids. One equivalent of $M(CO)_5THF$ (prepared by photolysis of 0.500 g of $W(CO)_6$ or 0.300 g of $Cr(CO)_6$) was reacted with 1 equiv of the tetraethylammonium salt of the phosphino acid. THF was removed from the reaction mixture by vacuum, and the resulting orange solid was washed three times with hexanes to yield an orange powder. Crystals were grown by the slow diffusion of hexane into a concentrated THF solution of the complex at −10 °C. Anal. Calcd for $[Et_4N][W(CO)_4(PPh_2CH_2CO_2)]$ (**5**) ($C_{22}H_{32}NO_6PW$): C, 42.53; H, 5.19; N, 2.25. Found: C, 43.87; H, 5.26; N, 2.32.

X-ray Crystallography. $[Et_4N][Cr(CO)_4(O_2CCH_2NRR')]$ Derivatives (1−3). Crystal data and details of data collection are given in Table 1. A yellow needle of **1**, a yellow-orange needle of **2**, and an orange block of **3** were mounted on glass fibers with epoxy cement at room temperature and cooled in a liquid nitrogen cold stream. Preliminary examination and data collection were performed on a Rigaku AFC5R X-ray diffractometer (Cu Kα, λ = 1.541 78 Å radiation) for **1** and a Nicolet R3m/v X-ray diffractometer (Mo Kα, λ = 0.710 73 Å radiation) for **2** and **3**. Cell parameters were calculated from the least-squares fitting of the setting angles for 24 reflections. Omega scans for several intense reflections indicated acceptable crystal quality. Data were collected for $4.0° \geq 2\theta \geq 50°$. Three control reflections, collected for every 97 reflections, showed no significant trends. Background measurements by stationary-crystal and stationary-counter techniques were taken at the beginning and end of each scan for half the total scan time. Lorentz and polarization corrections were applied to 1456 reflections for **1**, 3536 for **2**, and 3703 for **3**. A semiempirical absorption correction was applied to **1** and **3**. A total of 1456 unique reflections for **1**, 3391 for **2**, and 3520 for **3**, with $|I| \geq 2.0\sigma(I)$, were used in further calculations. All three structures were solved by direct methods [SHELXS program package, Sheldrick (1993)]. Full-matrix least-squares anisotropic refinement for all non-hydrogen atoms yielded R = 0.0745, R_w = 0.1943, and S = 1.042 for **1**, R = 0.0398, Rw = 0.0696, and S = 1.049 for **2**, and R = 0.0357, R_w = 0.0886, and S = 1.052 for **3**. Hydrogen atoms were placed in idealized positions with isotropic thermal parameters fixed at 0.08. Neutral-atom scattering factors and anomalous scattering correction terms were taken from *International Tables for X-ray Crystallography*.

$[Et_4N][W(CO)_4(O_2CCH(C(CH_3)_3)NH_2]$, 4. Crystal data and details of data collection are given in Table 1. An orange needle of **4** was mounted on a glass fiber with epoxy cement at room temperature and cooled in a liquid nitrogen cold stream. Preliminary examination and data collection were performed on a Rigaku AFC5R X-ray diffractometer (Cu Kα, λ = 1.541 78). Data collection methods and parameters are identical to those described for complexes **1**−**3**. Lorentz and polarization corrections were applied to 2711 reflections for **4**. A total of 2527 unique reflections were used in further calculations. Anisotropic refinement for all non-hydrogen atoms yielded R = 0.0590, R_w = 0.1381, and S = 1.103.

$[Et_4N][W(CO)_4(O_2CCH_2P(C_6H_5)_2]$, 5. Crystal data and details of data collection are given in Table 1. An orange needle of **5** was mounted on a glass fiber with epoxy cement at room temperature and

(6) (a) Tobe, M. L. *Adv. Inorg. Bioinorg. Mech.* **1983**, *2*, 1. (b) Garrick, F. J. *Nature (London)* **1937**, *139*, 507. (c) Dixon, N. E.; Jackson, W. G.; Marty, W.; Sargeson, A. M. *Inorg. Chem.* **1982**, *21*, 688. (d) Gaudin, M. J.; Clark, C. R.; Buckingham, D. A. *Inorg. Chem.* **1986**, *25*, 2569. (e) Buckingham, D. A.; Marzilli, P. A.; Sargeson, A. M. *Inorg. Chem.* **1969**, *8*, 1595. (f) Watson, A. A.; Prinsep, M. R.; House, D. A. *Inorg. Chim. Acta* **1986**, *115*, 95.

(7) Van Doorn, J. A.; Meijboom, N. *Phosphorus, Sulphur, Silicon* **1989**, *42*, 223.

Table 1. Crystallographic Data for Complexes **1**−**5**

	1	**2**	**3**	**4**	**5**
empirical formula	$C_{14}H_{24}N_2O_6Cr$	$C_{15}H_{26}N_2O_6Cr$	$C_{16}H_{28}N_2O_6Cr$	$C_{36}H_{64}N_4O_{12}W_2$	$C_{30}H_{40}NO_6PW$
FW	368.2	382.2	396.2	556.3	725.47
space group	$Pna2_1$	$P2_1/c$	$P2_1/c$	$P2_1$	$P2_1/c$
V, Å^3	1837.7(6)	1916.8(8)	1981.3(7)	2199.5(6)	3203.4(8)
Z	4	4	4	4	4
d_{calc}, g/cm^3	1.331	1.325	1.386	1.680	1.504
a, Å	13.622(3)	13.713(3)	11.558(2)	11.976(2)	17.101(2)
b, Å	13.029(3)	10.276(2)	11.519(2)	11.745(2)	13.310(2)
c, Å	10.354(2)	14.747(4)	14.964(3)	16.646(2)	14.130(2)
α, deg				90	90
β, deg		112.7(2)	96.00(3)	110.050(10)	95.120(10)
γ, deg				90	90
T, K	163	193	193	173	293
μ(Mo Kα), mm^{-1}	5.386	0.627	0.616	10.022	7.331
wavelength, Å	1.541 78	0.710 73	0.710 73	1.541 78	0.710 73
R_F,[a] %	7.45	3.98	3.57	5.90	3.24
R_{wF},[b] %	19.43	6.96	8.86	13.81	7.53

[a] $R_F = \sum|F_o - F_c|/\sum F_o$. [b] $R_{wF} = \{[\sum w(F_o^2 - F_c^2)^2]/(\sum wF_o^2)\}^{1/2}$.

Scheme 1

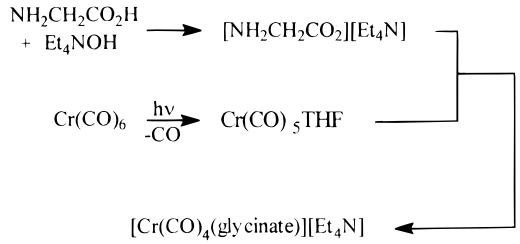

cooled in a liquid nitrogen cold stream. Preliminary examination and data collection were performed on a Nicolet R3m/v X-ray diffractometer (Mo Kα, $\lambda = 0.710\ 73$). Data collection methods and parameters are identical to those described for complexes **1**−**3**. Lorentz and polarization corrections were applied to 4980 reflections for **5**. A total of 4754 unique reflections were used in further calculations. Anisotropic refinement for all non-hydrogen atoms yielded $R = 0.0324$, $R_w = 0.0753$, and $S = 1.105$.

Kinetic Measurements. The rates of ^{13}CO exchange in these complexes were determined by placing an acetonitrile solution of the corresponding complex (0.6 mmol in 20 mL) under an atmosphere of ^{13}CO. The solution was situated in a thermostated water bath at 25.1 °C when M = Cr and at 40.0 °C when M = W and shaken periodically. The exchange process was monitored by observing the decrease in absorbance of the highest frequency ν(CO) band of the starting complex as a function of time.

Results

Synthesis. Each of these complexes was prepared in greater than 80% yield by the labile ligand displacement reaction of $M(CO)_5THF$, obtained *via* photolysis of $Cr(CO)_6$ or $W(CO)_6$, with the tetraethylammonium salt of the corresponding amino or phosphino acid in THF. Scheme 1 summarizes the general approach employed in the synthesis of the complexes under discussion, specifically indicating the preparation of the glycino complex of chromium. In each case examined, there was infrared spectral evidence that a metal pentacarbonyl intermediate preceded the production of the final isolated chelated product. With one exception, the sarcosine derivative, the neutral end of the ligand was observed to bind to the pentacarbonyl metal fragment initially. This was evident from the position of the ν(CO) bands and the separation (Δ) in $\nu(CO_2)$ asymmetric and symmetric modes (Table 2).[8] For example, in $Cr(CO)_5(NH_2CH_2CO_2)^-$ is 152 cm^{-1}, which is very close to that observed in the $[Et_4N][NH_2CH_2CO_2]$ salt, whereas Δ in $Cr(CO)_5(O_2CCH_2NHMe)^-$ is 233 cm^{-1}, which is more typical of monodentate carboxylate complexes. Similarly, the asymmetric and symmetric $\nu(CO_2)$ vibrations in the (N,O) chelated glycino complex which have been definitively assigned by ^{13}C labeling occur at 1622 and 1367 cm^{-1} with a corresponding Δ value of 255 cm^{-1}. On the other hand, these $\nu(CO_2)$ vibrational modes are observed at 1597 and 1395 cm^{-1} ($\Delta = 202$ cm^{-1}) in KBr, compatible with intermolecular hydrogen bonding between the distal oxygen atom of the carboxylate and the hydrogen atom of the amino group.

Table 3 lists the ^{13}C NMR data for the complexes in both the CO and carboxylate regions of the spectra. Chemical shift data for the $M(CO)_4$ moieties reveal a slight electronic difference between the CO ligand *trans* to oxygen versus the CO ligand *trans* to nitrogen. Furthermore, in the unsymmetrically substituted derivatives (i.e., sarcosine, **2**, and L-*tert*-leucine, **4**), ^{13}C NMR reveals that the axial carbonyls are no longer equivalent. The carboxylate ^{13}C resonances display small shifts relative to one another depending on the nature of the metal amino acid derivative.

The glycino complex of chromium, **1**, exhibits the antisymmetric and symmetric vibrations of the NH_2 group at 3365 and 3316 cm^{-1} in acetonitrile solution and at 3368 and 3173 cm^{-1} in KBr. These vibrational modes shift to 2294 and 2254 cm^{-1} in CH_3CN and 2288 and 2079 cm^{-1} in KBr upon forming the glycino-d_4 complex.[9] The greater difference in the $\nu(NH_2)$ frequencies noted in KBr most likely results from the extensive intermolecular hydrogen-bonding network found in the solid state (*vide infra*).

Structures. Crystals of **1** suitable for single-crystal X-ray structure determination were grown by slow diffusion of hexane into a concentrated THF solution of the complex over several days. The resulting crystals were small yellow needles that differed from the crystals of the tungsten analogue in several important aspects. The tungsten−glycine derivative grew long fibers up to 3.7 cm in length.[5] These latter crystals were considerably more stable than those of the chromium derivative described herein, the structure of which was determined at −110 °C to prevent loss of intensity of the signal. Finally, the tungsten analogue crystallized in the $P2_12_12_1$, space group, while complex **1** crystallized in $Pna2_1$. The difference in the two crystal structures can be found by carefully examining the packing diagrams of the two crystals. In tungsten, the glycinate ring packs so that it is *trans* to the glycinate rings in adjacent molecules; in chromium, the glycinate ring packs *cis* to other

(8) Nakamoto, K. *Infrared and Raman Spectra of Inorganic and Coordination Compounds*, 4th ed; Wiley: New York, 1986; p 231..

(9) Condrate, R. A.; Nakamoto, K. *J. Chem. Phys.* **1965**, *42*, 2590.

Table 2. Carbonyl Stretching Frequencies of $M(CO)_{4,5}$ Amino or Phosphino Acid Derivatives

complex[a]	ν(C≡O), cm^{-1}				ν(C=O), cm^{-1} asym	ν(C=O), cm^{-1} sym
$Cr(CO)_5(NH_2CH_2CO_2)^-$	2063 (w)	1928 (vs)	1861 (m)[b,c]		1621	1469
$Cr(CO)_5(O2CCH_2NHMe)^-$	2073 (w)	1908 (vs)	1863 (m)[b,d]		1627	1394
$Cr(CO)_5(NMe_2CH_2CO_2)^-$	2063 (w)	1923 (vs)	1862 (m)[b,c]		1636	1469
$W(CO)_5(NH_2CH(t\text{-}Bu)CO_2)^-$	2061 (w)	1913 (vs)[b,c]			1636	1469
$W(CO)_5(NH_2CH(C_6H_5)CO_2)^-$	2062 (w)	1918 (vs)[b,c]			1646	1469
$Cr(CO)_5(P(C_6H_5)2CH_2CO_2)^-$	2069 (w)	1928 (vs)[b,e]			1614	1486
$W(CO)_5(P(C_6H_5)2CH_2CO_2)^-$	2062 (w)	1934 (vs)[b,e]			1614	1486
$Cr(CO)_4(O_2CCH_2NH_2)^-$	1999 (w)	1867 (vs)	1856 (sh)	1800 (m)[f]	1622	1367
$Cr(CO)_4(O_2{}^{13}CCH_2NH_2)^-$	1998 (w)	1868 (vs)	1857 (sh)	1800 (m)[f]	1579	1321
$Cr(CO)_4(O_2CCH_2NHMe)^-$	1999 (w)	1866 (vs)	1855 (sh)	1803 (m)[f]	1627	1367
$Cr(CO)_4(O_2CCH_2NMe_2)^-$	1999 (w)	1866 (vs)	1853 (sh)	1807 (m)[f]	1632	1378
$W(CO)_4(O_2CCH(t\text{-}Bu)NH_2)^-$	1993 (w)	1855 (vs)	1842 (sh)	1795 (m)[f]	1621	1363
$W(CO)_4(NH_2CH(C_6H_5)CO_2)^-$	1996 (w)	1856 (vs)	1844 (sh)	1799 (m)[f]	1643	1374
$Cr(CO)_4(P(C_6H_5)_2CH_2CO_2)^-$	2003 (w)	1881 (vs)	1862 (sh)	1816 (m)[f]	1635	1374
$W(CO)_4(P(C_6H_5)_2CH_2CO_2)^-$	2004 (w)	1875 (vs)	1856 (sh)	1814 (m)[f]	1631	1376

[a] As the tetraethylammonium salt. [b] Spectra determined in THF. [c] Nitrogen-bound complex. [d] Oxygen-bound complex. [e] Phosphorus-bound complex. [f] Spectra determined in CH_3CN.

Table 3. ^{13}C NMR Data for the Carbonyl and Carboxylate Ligands in $M(CO)_4(O_2CCHXNRR')^-$ Anions[a]

complex[b]	^{13}C resonance, ppm[c] CO (axial)	CO (*trans* to N)	COz (*trans* to O)	CO_2^-
$Cr(CO)_4(O_2CCH_2NH_2)^-$	215.1	229.0	229.5	184.5
$Cr(CO)_4(O_2CCH_2NHMe)^-$	215.8, 215.4	230.2	230.3	185.7
$Cr(CO)_4(O_2CCH_2NMe_2)^-$	214.1	228.8	230.0	176.6
$W(CO)_4(O_2CCH(t\text{-}Bu)NH_2)^-$	205.8, 205.7	216.2	217.0	179.5

[a] Spectra determined in acetonitrile-d_3. [b] As the tetraethylammonium salt. [c] The assignments of the ^{13}C signals for CO groups *trans* to N *vs* those *trans* to O are based on the general observation that the ^{13}C resonance for a CO group *trans* to N is upfield relative to a CO group *trans* to O in $W(CO)_5$ derivatives (see, e.g.: Todd, L. J.; Wilkinsin, J. R. *J. Organomet. Chem.* **1974**, *77*, 1. Reference: Darensbourg, D. J.; Wiegreffe, H. P. *Inorg. Chem.* **1990**, *29*, 592.). Nevertheless, the signals are quite close and an absolute distinction is not needed at this time.

rings. A comparison of the packing diagrams for the two metal systems is shown in Figure 1. Figure 2 shows a thermal ellipsoid diagram of the anion of complex **1**, and selected bond lengths and bond angles are shown in Table 4. The structure of complex **1** consists of a glycinate residue that forms a chelate ring at the metal tetracarbonyl center through its nitrogen atom and one of its oxygen atoms to give a distorted octahedron. The Cr−N bond length was determined to be 2.15(1) Å while the Cr−O bond length was 2.14(1) Å. The glycinate ligand formed a 77.6(5)° bite angle with the metal atom.

The crystal structure of **1** reveals strong intermolecular hydrogen bonds formed between the N−H group of a glycinate ligand in one anion and the distal oxygen of the carboxylate group in an adjacent anion. As expected, the glycino chromium derivative mimics the glycino tungsten derivative in that hydrogen bonding holds the complexes together in infinite helical chains, with each turn of the helix consisting of three metal anions (Figure 3). Free glycine crystallizes in three distinct forms: α, β, and γ.[10] Each displays extensive intermolecular hydrogen bonding, with the γ form being composed of infinite helical chains packed together with lateral hydrogen bonding between the chains forming a three-dimensional network of hydrogen bonds. Table 5 lists typical bond lengths of the three forms of glycine and the chromium-bound glycinate. In Table 6, typical N···O distances for the these different forms of hydrogen-bound glycine are provided.

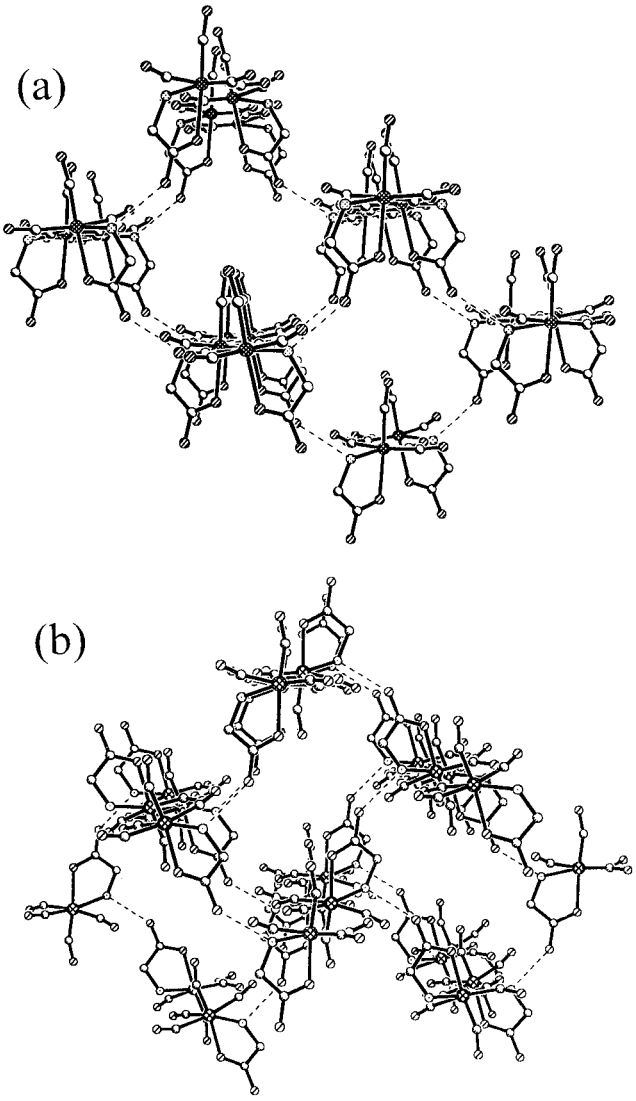

Figure 1. (a) Cr glycinate packing diagram. (b) W glycinate packing diagram.

In a manner analogous to that employed for complex **1**, single crystals of $[Et_4N][Cr(CO)_4(O_2CCH_2NHMe)]$ (**2**) and $[Et_4N][Cr(CO)_4(O_2CCH_2NMe_2)]$ (**3**) were obtained by slow diffusion of hexane into a concentrated THF solution of the respective

(10) (a) Marsh, R. E. *Acta Crystallogr.* **1958**, *11*, 654. (b) Power, L. F.; Turner, K. E.; Moore, F. H. *Acta Crystallogr., Sect. B* **1976**, *11*, 32. (c) Iitaka, Y. *Acta Crystallogr.* **1960**, *13*, 35. (d) Iitaka, Y. *Acta Crystallogr.* **1961**, *14*,

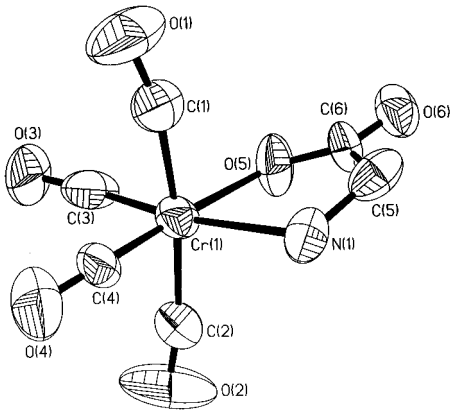

Figure 2. ORTEP diagram of the anion of complex **1**, showing 50% probability thermal motion ellipsoids with atomic numbering scheme.

Table 4. Selected Bond Lengths (Å) and Angles (deg) for $[Et4][Cr(CO)_4(O_2CCH_2NH_2)]$ (**1**)[a]

Cr(1)−C(1)	1.83(2)	Cr(1)−O(5)	2.219(13)
Cr(1)−C(2)	1.89(2)	O(5)−C(5)	1.20(2)
Cr(1)−C(3)	1.819(14)	O(6)−C(5)	1.25(2)
Cr(1)−C(4)	1.73(2)	N(1)−C(6)	1.49(2)
Cr(1)−N(1)	2.150(10)		
C(4)−Cr(1)−C(3)	90.6(11)	C(2)−Cr(1)−O(5)	92.6(9)
C(4)−Cr(1)−C(1)	86.1(8)	N(1)−Cr(1)−O(5)	75.1(5)
C(3)−Cr(1)−C(1)	88.0(6)	C(5)−O(5)−Cr(1)	117.0(10)
C(4)−Cr(1)−C(2)	87.9(11)	C(6)−N(1)−Cr(1)	110.6(9)
C(3)−Cr(1)−C(2)	86.2(7)	O(5)−C(5)−O(6)	123.1(14)
C(1)−Cr(1)−C(2)	171.5(8)	O(5)−C(5)−C(6)	118.9(13)
C(4)−Cr(1)−N(1)	100.3(6)	O(6)−C(5)−C(6)	117.9(12)
C(3)−Cr(1)−N(1)	168.8(10)	C(5)−C(6)−N(1)	113.9(12)
C(1)−Cr(1)−N(1)	90.2(5)	O(2)−C(2)−Cr(1)	171(2)
C(2)−Cr(1)−N(1)	96.7(6)	O(4)−C(4)−Cr(1)	173(2)
C(4)−Cr(1)−O(5)	175.4(6)	O(1)−C(1)−Cr(1)	167(2)
C(3)−Cr(1)−O(5)	94.0(10)	O(3)−C(3)−Cr(1)	169(3)
C(1)−Cr(1)−O(5)	93.9(7)		

[a] Estimated standard deviations are given in parentheses.

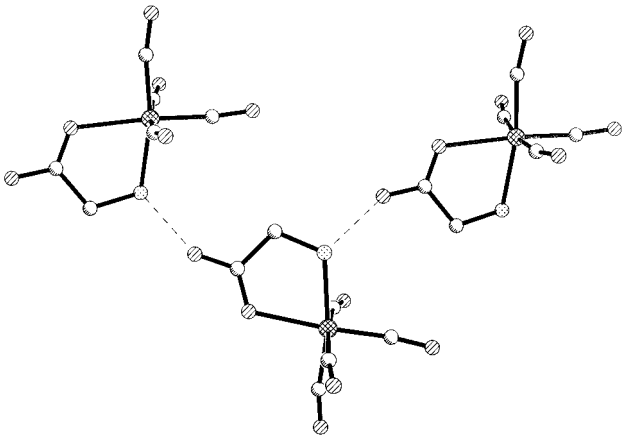

Figure 3. Ball and stick representation of the anion of complex **1** illustrating the intermolecular hydrogen bonding which forms helical chains.

complex. Figure 4 shows a thermal ellipsoid drawing of **2**, with selected bond lengths and angles listed in Table 7. Like complex **1**, the sarcosine derivative exists in a polymeric structure in which adjoining molecules are hydrogen bound through the carboxylate oxygen and the amine nitrogen. The hydrogen bonding is somewhat weaker here, however, as seen by a N···O distance of 2.82. Not surprisingly, therefore, the crystal structure of **2** shows it to be completely analogous to that of **1**, with Cr−N and Cr−O bond lengths of 2.146(2) and 2.090(2) Å, respectively, and a bite angle of 77.75(8)°. The

Table 5. Selected Internal Bond Distances (Å) in Free and Bound Glycine[a]

glycine form	N−C1	C1−C2	C2−O1	C2−O2
Cr−glycinate	1.50(2)	1.47(2)	1.24(2)	1.24(2)
W−glycinate	1.43(4)	1.50(4)	1.32(4)	1.38(4)
α	1.474(5)	1.523(5)	1.252(5)	1.255(5)
β	1.484(15)	1.521(15)	1.233(15)	1.257(15)
γ	1.491(11)	1.527(11)	1.237(11)	1.254(11)

[a] Estimated standard deviations are given in parentheses. Atom-numbering scheme:

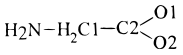

Table 6. Hydrogen-Bonding Distances (Å) in Free and Bound Glycine

glycine form	N···O (Å)	ref
Cr−glycinate	2.828	this work
W−glycinate	2.746	5
α	2.768	10a, 10b
β	2.758	10c
γ	2.687	10d

Table 7. Selected Bond Lengths (Å) and Angles (deg) for $[Et_4N][Cr(CO)_4(O_2CCH_2NHMe)]$ (**2**)[a]

Cr(1)−C(1)	1.894(3)	O(1)−C(1)	1.154(3)
Cr(1)−C(2)	1.887(3)	O(4)−C(4)	1.165(3)
Cr(1)−C(3)	1.828(3)	O(5)−C(5)	1.261(3)
Cr(1)−C(4)	1.805(3)	O(6)−C(5)	1.234(3)
Cr(1)−O(5)	2.091(2)	N(1)−C(7)	1.469(3)
Cr(1)−N(1)	2.146(2)	N(1)−C(6)	1.476(3)
O(2)−C(2)	1.159(3)	C(5)−C(6)	1.510(4)
O(3)−C(3)	1.163(3)		
C(4)−Cr(1)−C(3)	89.94(13)	O(5)−Cr(1)−N(1)	77.73(8)
C(4)−Cr(1)−C(2)	86.45(13)	C(5)−O(5)−Cr(1)	117.8(2)
C(3)−Cr(1)−C(2)	86.47(12)	C(7)−N(1)−C(6)	111.9(2)
C(4)−Cr(1)−C(1)	84.63(13)	C(7)−N(1)−Cr(1)	115.8(2)
C(3)−Cr(1)−C(1)	86.27(12)	C(6)−N(1)−Cr(1)	106.7(2)
C(2)−Cr(1)−C(1)	168.50(13)	O(2)−C(2)−Cr(1)	170.7(3)
C(4)−Cr(1)−O(5)	174.93(11)	O(3)−C(3)−Cr(1)	177.7(3)
C(3)−Cr(1)−O(5)	95.12(10)	O(1)−C(1)−Cr(1)	169.0(3)
C(2)−Cr(1)−O(5)	93.46(11)	O(4)−C(4)−Cr(1)	177.9(3)
C(1)−Cr(1)−O(5)	96.06(11)	O(6)−C(5)−O(5)	124.8(3)
C(4)−Cr(1)−N(1)	97.24(11)	O(6)−C(5)−C(6)	119.4(3)
C(3)−Cr(1)−N(1)	172.33(11)	O(5)−C(5)−C(6)	115.7(3)
C(2)−Cr(1)−N(1)	96.66(11)	N(1)−C(6)−C(5)	111.3(2)
C(1)−Cr(1)−N(1)	91.67(11)		

[a] Estimated standard deviations are given in parentheses.

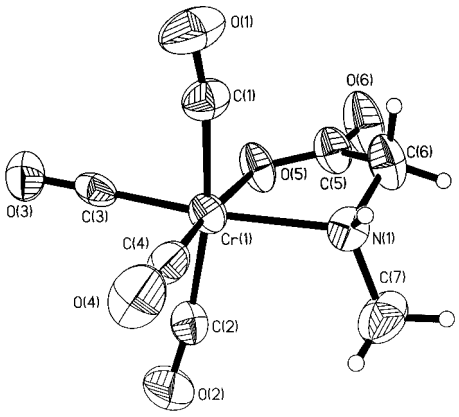

Figure 4. ORTEP diagram of the anion of complex **2**, showing 50% probability thermal motion ellipsoids with atomic numbering scheme.

bond lengths for complex **2** are more accurate than those determined for complex **1** and hence allow for comparison among metal carbon distances. In this regard the average Cr−C_{ax} bonds at 1.891(3) Å are longer than the average Cr−C_{eq}

Table 8. Selected Bond Lengths (Å) and Angles (deg) for $[Et_4N][Cr(CO)_4(O_2CCH_2NMe_2)]$ (**3**)[a]

Cr(1)−C(1)	1.890(2)	O(1)−C(1)	1.150(3)
Cr(1)−C(2)	1.886(3)	O(4)−C(4)	1.160(3)
Cr(1)−C(3)	1.824(3)	O(5)−C(5)	1.260(3)
Cr(1)−C(4)	1.820(3)	O(6)−C(5)	1.239(3)
Cr(1)−O(5)	2.080(2)	N(1)−C(6)	1.458(3)
Cr(1)−N(1)	2.193(2)	N(1)−C(7)	1.476(3)
O(3)−C(3)	1.158(3)	N(1)−C(8)	1.476(3)
O(2)−C(2)	1.150(3)	C(5)−C(6)	1.523(4)
C(4)−Cr(1)−C(3)	91.20(12)	C(5)−O(5)−Cr(1)	118.4(2)
C(4)−Cr(1)−C(2)	84.02(11)	C(6)−N(1)−C(7)	108.7(2)
C(3)−Cr(1)−C(2)	84.81(12)	C(6)−N(1)−C(8)	110.0(2)
C(4)−Cr(1)−C(1)	82.53(11)	C(7)−N(1)−C(8)	107.5(2)
C(3)−Cr(1)−C(1)	86.78(10)	C(6)−N(1)−Cr(1)	104.34(14)
C(2)−Cr(1)−C(1)	163.97(11)	C(7)−N(1)−Cr(1)	111.6(2)
C(4)−Cr(1)−O(5)	176.02(9)	C(8)−N(1)−Cr(1)	114.6(2)
C(3)−Cr(1)−O(5)	92.67(9)	O(3)−C(3)−Cr(1)	178.9(2)
C(2)−Cr(1)−O(5)	95.40(9)	O(2)−C(2)−Cr(1)	168.7(2)
C(1)−Cr(1)−O(5)	98.61(9)	O(1)−C(1)−Cr(1)	168.1(2)
C(4)−Cr(1)−N(1)	99.52(10)	O(4)−C(4)−Cr(1)	178.0(2)
C(3)−Cr(1)−N(1)	169.22(10)	O(6)−C(5)−O(5)	125.0(2)
C(2)−Cr(1)−N(1)	97.39(10)	O(6)−C(5)−C(6)	120.2(2)
C(1)−Cr(1)−N(1)	93.40(9)	O(5)−C(5)−C(6)	114.7(2)
O(5)−Cr(1)−N(1)	76.64(7)	N(1)−C(6)−C(5)	111.1(2)

[a] Estimated standard deviations are given in parentheses.

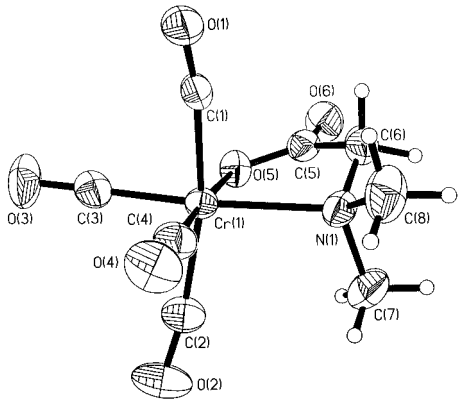

Figure 5. ORTEP diagram of the anion of complex **3**, showing 50% probability thermal motion ellipsoids with atomic numbering scheme.

bonds determined to be 1.817(3) Å; there is no significant difference, however, between the Cr−C bonds for CO groups alternately *trans* to nitrogen or oxygen (1.828(3) and 1.805(3) Å, respectively).

Complex **3** crystallized as an orange block instead of a needle as in complexes **1** and **2**. In these latter two complexes, the glycinate ring is capable of intermolecular hydrogen-bond formation. This is not possible in crystals of the tetraethylammonium salt of the dimethylamino carboxylate chromium tetracarbonyl. Pertinent bond lengths and angles are provided in Table 8. Similar to complexes **1** and **2**, the dimethylglycine derivative exists as a distorted octahedron. Figure 5 contains a thermal ellipsoid diagram of **3**. The axial carbonyls have an average Cr−C−O bond angle of 168.4(2)° and an average Cr−C bond length of 1.888(3) Å. The carboxylate and amine groups exhibit a small *trans* effect, giving equatorial Cr−C bond lengths of 1.820 Å (*trans* to nitrogen) and 1.824 Å (*trans* to oxygen). The Cr−N and Cr−O bond lengths of 2.193(2) and 2.080(2) Å are similar to those for complexes **1** and **2**. The bite angle, at 76.64(7)°, is also similar to the bite angles of the glycine and sarcosine derivatives.

Crystals of **4** ($[Et_4N][W(CO)_4(O_2CCH(C(CH_3)_3)NH_2)]$) and **5** ($[Et_4N][W(CO)_4(O_2CCH_2P(C_6H_5)_2)]$) were also grown from the slow diffusion of hexane into a concentrated THF solution

Table 9. Selected Bond Lengths (Å) and Angles (deg) for $[Et_4N][W(CO)_4(O_2CCH(C(CH_3)_3NH_2)]$ (**4**)[a]

W(1)−C(1)	1.91(3)	O(6)−C(5)	1.21(3)
W(1)−C(2)	2.05(3)	N(1)−C(6)	1.51(4)
W(1)−C(3)	1.81(3)	C(5)−C(6)	1.44(4)
W(1)−C(4)	1.88(3)	C(6)−C(7)	1.63(4)
W(1)−O(5)	2.18(2)	C(7)−C(8)	1.57(4)
W(1)−N(1)	2.32(2)	C(7)−C(9)	1.52(4)
O(5)−C(5)	1.33(4)	C(7)−C(10)	1.48(4)
C(3)−W(1)−C(4)	86(2)	O(1)−C(1)−W(1)	169(3)
C(3)−W(1)−C(1)	89(2)	O(2)−C(2)−W(1)	168(3)
C(4)−W(1)−C(1)	84(2)	O(3)−C(3)−W(1)	175(3)
C(3)−W(1)−C(2)	84.2(12)	O(4)−C(4)−W(1)	173(4)
C(4)−W(1)−C(2)	87.9(14)	O(6)−C(5)−O(5)	121(3)
C(1)−W(1)−C(2)	169.6(13)	O(6)−C(5)−C(6)	123(3)
C(3)−W(1)−O(5)	98.2(12)	O(5)−C(5)−C(6)	116(3)
C(4)−W(1)−O(5)	175.8(13)	C(5)−C(6)−N(1)	114(3)
C(1)−W(1)−O(5)	95.7(12)	C(5)−C(6)−C(7)	118(2)
C(2)−W(1)−O(5)	93.1(11)	N(1)−C(6)−C(7)	106(2)
C(3)−W(1)−N(1)	170.8(12)	C(10)−C(7)−C(9)	110(2)
C(4)−W(1)−N(1)	103.2(13)	C(10)−C(7)−C(8)	108(3)
C(1)−W(1)−N(1)	91.9(11)	C(9)−C(7)−C(8)	109(2)
C(2)−W(1)−N(1)	95.9(11)	C(10)−C(7)−C(6)	114(2)
O(5)−W(1)−N(1)	72.7(9)	C(9)−C(7)−C(6)	110(3)
C(5)−O(5)−W(1)	119(2)	C(8)−C(7)−C(6)	106(2)
C(6)−N(1)−W(1)	106(2)		

[a] Estimated standard deviations are given in parentheses.

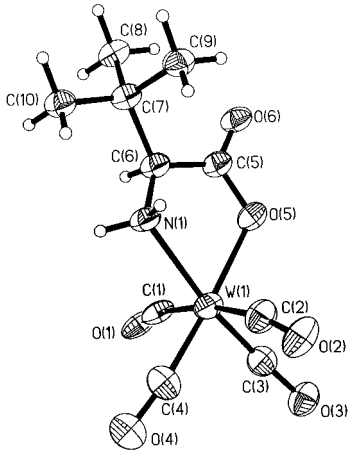

Figure 6. ORTEP diagram of the anion of complex **4**, showing 50% probability thermal motion ellipsoids with atomic numbering scheme.

of the appropriate complex over several days and exhibit the slightly distorted octahedral geometry observed for **1**−**3**. Yellow-orange needles in the space group $P2_1$ were obtained for **4**. Two independent anions and cations were observed in the unit cell of **4**; similar bond distances and angles are seen in the two independent anions. Table 9 lists selected bond lengths and angles, while Figure 6 shows a thermal ellipsoid drawing of the anion of **4**. The bite angle is found to be 72.6 °C, which is entirely consistent with the bite angles observed for the $W(CO)_4(glycinate)^-$ derivatives. Similar to complexes **1** and **2**, intermolecular hydrogen bonding is observed between the distal oxygen and the amine N−H group, albeit somewhat weaker here, where the N···O distance is 2.859 Å. The phosphino complex **5** crystallized in large orange blocks in the space group $P2_1/c$. A molecule of THF cocrystallized with the complex. The phosphinate ligand forms a bite angle of 75.0° with the metal atom. Important bond lengths and angles are in Table 10, while in Figure 7 there is a thermal ellipsoid diagram of the anion of **5**.

Reactivity Studies. Preliminary data with regard to CO ligand lability in tungsten tetracarbonyl amino acid derivatives have revealed a greatly enhanced rate of CO dissociation in the

Table 10. Selected Bond Lengths (Å) and Angles (deg) for $[Et_4N][W(CO)_4(O_2CCH_2P(C_6H_5)_2)]$ (**5**)[a]

W(1)−C(1)	2.010(6)	C(7)−C(8)	1.376(7)
W(1)−C(2)	2.020(6)	C(7)−C(12)	1.391(7)
W(1)−C(3)	1.970(6)	C(8)−C(9)	1.378(8)
W(1)−C(4)	1.959(6)	C(9)−C(10)	1.361(9)
W(1)−O(6)	2.237(3)	C(10)−C(11)	1.353(9)
W(1)−P(1)	2.5021(13)	C(11)−C(12)	1.399(8)
P(1)−C(5)	1.834(5)	C(13)−C(18)	1.383(8)
P(1)−C(7)	1.816(5)	C(13)−C(14)	1.384(8)
P(1)−C(13)	1.811(5)	C(14)−C(15)	1.391(8)
O(5)−C(6)	1.234(6)	C(15)−C(16)	1.381(10)
O(6)−C(6)	1.279(6)	C(16)−C(17)	1.352(11)
C(5)−C(6)	1.518(6)	C(17)−C(18)	1.390(8)

C(4)−W(1)−C(3)	90.3(2)	C(5)−P(1)−W(1)	100.3(2)
C(4)−W(1)−C(1)	85.8(2)	C(6)−O(6)−W(1)	127.0(3)
C(3)−W(1)−C(1)	91.4(2)	O(3)−C(3)−W(1)	178.5(6)
C(4)−W(1)−C(2)	86.5(2)	O(1)−C(1)−W(1)	175.5(5)
C(3)−W(1)−C(2)	89.1(2)	O(6)−C(6)−C(5)	117.6(4)
C(1)−W(1)−C(2)	172.3(2)	C(8)−C(7)−C(12)	117.7(5)
C(4)−W(1)−O(6)	175.8(2)	C(8)−C(7)−P(1)	119.9(4)
C(3)−W(1)−O(6)	93.8(2)	C(12)−C(7)−P(1)	122.3(4)
C(1)−W(1)−O(6)	93.6(2)	C(7)−C(8)−C(9)	121.7(6)
C(2)−W(1)−O(6)	94.1(2)	C(10)−C(9)−C(8)	119.7(6)
C(4)−W(1)−P(1)	100.9(2)	C(11)−C(10)−C(9)	120.6(6)
C(3)−W(1)−P(1)	168.7(2)	C(10)−C(11)−C(12)	120.1(6)
C(1)−W(1)−P(1)	90.1(2)	C(7)−C(12)−C(11)	120.2(6)
C(2)−W(1)−P(1)	90.9(2)	C(14)−C(13)−P(1)	120.7(4)
O(6)−W(1)−P(1)	74.97(9)	C(13)−C(14)−C(15)	120.4(6)
C(13)−P(1)−C(7)	103.7(2)	C(16)−C(15)−C(14)	119.3(7)
C(13)−P(1)−C(5)	105.1(2)	C(17)−C(16)−C(15)	120.4(7)
C(13)−P(1)−W(1)	124.2(2)	C(13)−C(18)−C(17)	119.4(7)
C(7)−P(1)−W(1)	116.5(2)		

[a] Estimated standard deviations are given in parentheses.

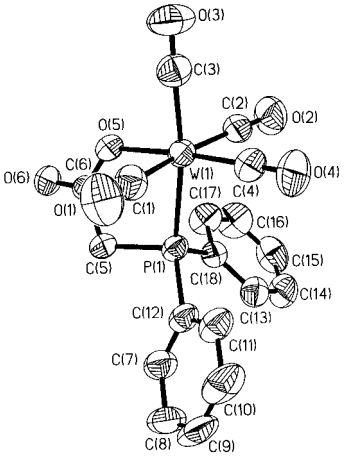

Figure 7. ORTEP diagram of the anion of complex **5**, showing 50% probability thermal motion ellipsoids with atomic numbering scheme.

glycino and sarcosino derivatives relative to the *N*,*N*-dimethylglycino complex. It was suggested that this rate increase was due to the formation of a transient, substitutionally labile amido complex resulting from deprotonation of the amine functionality (see Scheme 2).[5] Generation of the amido intermediate, the rate-determining step in the substitution reaction, is assisted by the stabilization resulting from π-donation by the amido ligand to the coordinatively unsaturated metal center. Indeed, it is well established that amido ligands are good π-donating ligands, and hence good CO-labilizing groups. This process is proposed to be analogous to that well documented for the base-assisted substitution reaction of the cobalt ammine complex outlined in Scheme 3.[6]

Although the lack of CO lability in the *N*,*N*-dimethylglycino derivative provides indirect evidence for this proposal, we have endeavored herein to obtain direct evidence in support of

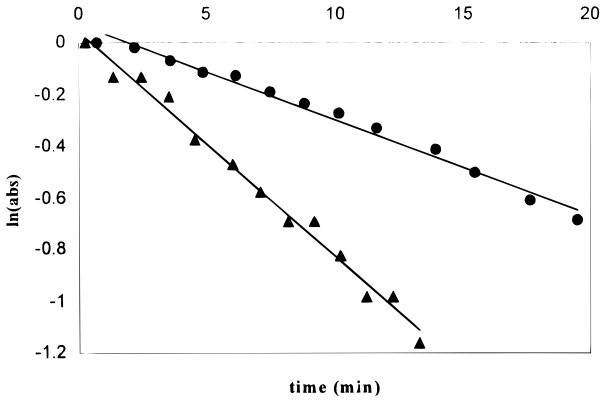

Figure 8. The isotope effect for $W(CO)_4$(glycinate)$^-$ at 40 °C: k_H (▲) = 1.43 × 10^{-3} s^{-1}, k_D (●) = 6.11 × 10^{-4} s^{-1}, k_H/k_D = 2.34.

Scheme 2

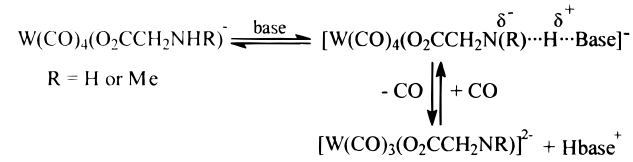

Scheme 3

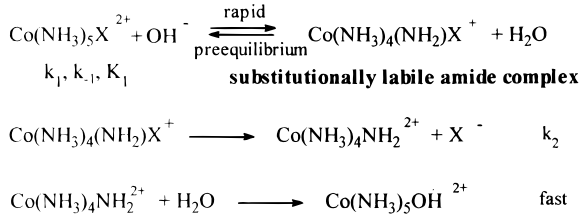

Table 11. Temperature Dependent Rate Constant Data for CO Exchange in the $W(CO)_4$(glycinate)$^-$ Anion

temp (K)	k, s^{-1}
293	0.000 271
298	0.000 506
303	0.000 626
307	0.000 928
313	0.001 47
318	0.002 70

Scheme 2. In such a process which involves N−H bond breakage with concomitant CO dissociation and metal−nitrogen multiple bond formation, it is anticipated that there will be a significant deuterium isotope effect. Relevant to this we have synthesized the glycino-d_4 complex of tungsten tetracarbonyl and measured the rate of CO ligand exchange in this isotopomer with that previously reported for the $W(CO)_4(O_2CCH_2NH_2)^-$ anion (eq 3). Indeed, as is readily seen from the raw data in

$$W(CO)_4(O_2CCH_2NH_2)^- + {}^{13}CO \rightleftharpoons W(CO)_3({}^{13}CO)(O_2CCH_2NH_2)^- + {}^{12}CO \quad (3)$$

Figure 8, the nondeuterated glycino complex undergoes CO exchange with a first-order rate constant 2.34 times greater than the corresponding value determined for its deuterated analog, 1.43 × 10^{-3} s^{-1} *vs* 6.11 × 10^{-4} s^{-1} at 40 °C. Consistent with this observation, the NH_2 linkage was observed to undergo facile exchange with D_2O in acetonitrile on a similar time scale. The activation parameters determined from the temperature dependent rate constant data listed in Table 11 for the reaction in eq 3 ($\Delta H^{\ddagger}$ = 15.4 ± 1.0 kcal/mol and $\Delta S^{\ddagger}$ = −23.2 ± 3.2 eu) are also consistent with a concomitant bond-making/bond-breaking

process.[11] It is important to note here that we have previously ruled out the CO substitution pathway which involves chelate ring-opening with concomitant formation of a pentacarbonyl species which subsequently undergoes CO dissociation.[5] This was accomplished by an *in situ* high-pressure ^{13}C NMR experiment employing ^{13}CO where the pentacarbonyl derivative ($W(CO)_5O_2CCH_2NH_2^-$ or $W(CO)_5NH_2CH_2CO_2^-$) was not detected. Indeed the rate of CO exchange in $W(CO)_4(O_2CCH_2NH_2)^-$ is faster than that anticipated for CO loss in either tungsten pentacarbonyl isomer.

In order to further add credibility to the proposed mechanism (Scheme 2), we have examined the effect of substituents at the methylene carbon atom of the glycine ligand. That is, the rate constants for intermolecular CO ligand exchange in the complexes $[Et_4N][W(CO)_4(O_2CCH(C(CH_3)_3)NH_2)]$ and $[Et_4N][W(CO)_4(O_2CCH(C_6H_5)NH_2)]$ were determined in acetonitrile to be 2.16×10^{-3} s^{-1} and 1.38×10^{-3} s^{-1}, respectively. Upon comparing these data with the similar CO exchange rate constant found for the glycino complex (1.47×10^{-3} s^{-1}), it is clear that substitution at the methylene carbon atom by either electron-donating or -withdrawing substituents has only a small effect on the rate of the CO exchange process. On the other hand, substituents on the nitrogen atom have a much greater influence on this process. This is not surprising since the inductive effects of these substituents on the loss of the N−H proton, and subsequent interaction of the amido group with the metal center, are expected to be small. On the other hand, these small rate changes may be the result of steric influences, where the relief of steric strain in the more hindered *tert*-butyl derivative accounts for the more facile CO dissociation. Indeed, the greater steric encumbance of the *tert*-leucinate ligand *vs* the glycinate ligand is manifested in a longer intermolecular N···O bond distance resulting from hydrogen-bond formation in the *tert*-leucinate tungsten complex (2.859 Å) *vs* 2.746 Å in the glycinate derivative. Furthermore, upon replacing the NH_2 group with PPh_2 the rate constant measured for CO exchange at 25 °C dramatically changed from 5.06×10^{-4} s^{-1} to 5.37×10^{-6} s^{-1}. This latter observation was anticipated on the basis of the fact that dissociative CO loss in the $W(CO)_5O_2CCH_3^-$ anion, which occurs with a $k = 6.4 \times 10^{-4}$ s^{-1} at 25 °C, is greatly retarded upon replacing a CO ligand with a phosphine ligand.[12]

The rates of CO exchange in anionic chromium pentacarbonyl derivatives are intrinsically quite fast. For example, dissociative CO ligand substitution in $Cr(CO)_5O_2CCH_3^-$ occurs with a rate constant of 1.81×10^{-2} s^{-1} at 25 °C. Hence, it would be expected that CO substitution in amino acid derivatives of chromium carbonyl would be very facile. Indeed, this is the case for all three chromium glycino complexes (derived from glycine, sarcosine, and dimethylglycine) where CO exchange with free ^{13}CO in solution is observed at ambient temperature with rate constant values of 6.4×10^{-3}, 5.0×10^{-3}, and 4.4×10^{-3} s^{-1}, respectively, at 25 °C. Although the kinetic effect of an amido intermediate is overshadowed by the innate CO lability exhibited in these chromium analogues, the trends noted are nevertheless similar to those observed in the corresponding tungsten derivatives. That is, the $Cr(CO)_5O_2CCH_3^-$ anion's rate constant for dissociative CO loss is somewhat greater than that seen in the glycino derivatives, where $k_{glycine} > k_{sarcosine} > k_{dimethylglycine}$. Similarly, CO dissociation in the phosphino derivative, $[Et_4N][Cr(CO)_4O_2CCH_2PPh_2]$, is more greatly inhibited relative to that in the $Cr(CO)_5O_2CCH_3^-$ anion than is the corresponding process involving the glycino derivatives. For example, in the phosphino derivative the rate constant at 25 °C for intermolecular CO exchange was determined to be 3.94×10^{-4} s^{-1}.

It was possible to spectroscopically observe a solvated intermediate during the CO substitution process involving complex **1** in CH_3CN or THF. For example, when argon is bubbled through an acetonitrile solution of **1**, the four bands listed in Table 2 are gradually replaced by two new bands which appear at 1896.9 (s) and 1749.3 (vs) cm^{-1} in an intensity pattern of a tricarbonyl species of local C_{3v} symmetry. The ^{13}C NMR of the tricarbonyl derivative in CD_3CN at ambient temperature reveals a peak at 234.4 ppm. Upon cooling of this solution to −40 °C, this peak resolves into three peaks at 236.5, 233.8, and 233.7 ppm. This is analogous to what has been found in the tungsten−glycinate complex, although the carbonyls in that system were found to be static at ambient temperature. It is assumed that this tricarbonyl anion contains a solvent molecule (in this instance CD_3CN) in the metal's coordination sphere. While there is precedent for coordinatively unsaturated group 6 metal carbonyl derivatives in the literature, both the tungsten and chromium glycinate complexes are unique in that they lack strongly π-donating ligands such as aryloxides. Reaction 4 is readily reversible upon the addition of an atmosphere of CO, as shown by ν(CO) infrared spectroscopy.

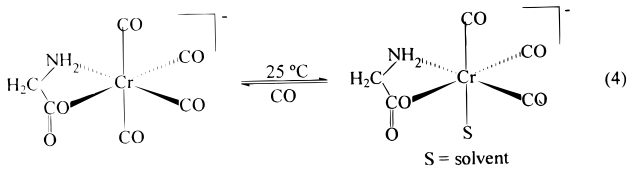

(4)

Summary

Herein we have provided additional examples of stable organometallic complexes containing amino carboxylate groups derived from both natural and unnatural amino acids.[13−16] As has been generally observed for metal complexes in higher oxidation states, the amino carboxylate group is bound to the zero-valent group 6 metal centers *via* one oxygen atom of the carboxylate group and the α-amino functionality.[17] This coordination mode of α-amino carboxylates to a wide variety of transition metals is most common due to the formation of a thermodynamically highly favored five-membered ring.

Investigations of the enhanced CO lability exhibited by some select amino carboxylates of tungsten carbonyl clearly point to a mechanism which involves N−H hydrogen abstraction to concomitantly afford a CO-labilizing amido functionality. However, the innate lability of the CO ligands in carboxylate derivatives of chromium carbonyl masks the secondary effect resulting from formation of the amido intermediates in these instances. This proposed mechanism is consistent with the labilizing properties observed in structurally characterized amido derivatives of tungsten carbonyl, i.e., $W(CO)_3(OC_6H_4NH)_2^-$ and $W(CO)_3(NHC_6H_4NH)_2^-$. Support for this conclusion is based on the lack of this effect in the absence of the N−H functionality

(11) (a) Darensbourg, D. J. *Adv. Organomet. Chem.* **1982**, *21*, 113. (b) Howell, J. A. S.; Burkinshaw, P. M. *Chem. Rev.* **1983**, *83*, 557 and references therein.
(12) Darensourg, D. J.; Joyce, J. A.; Bischoff, C. J.; Reibenspies, J. H. *Inorg. Chem.* **1991**, *30*, 1137.
(13) Meder, H.-J.; Beck, W. *Z. Naturforsch.* **1986**, *41B*, 1247.
(14) Petri, W.; Beck, W. *Chem. Ber.* **1984**, *117*, 3265.
(15) Grotjahn, D. B.; Groy, T. L. *J. Am. Chem. Soc.* **1994**, *116*, 6969.
(16) Schubert, U.; Tewinkel, S.; Möller, F. *Inorg. Chem.* **1995**, *34*, 995.
(17) Laurie, S. H. In *Comprehensive Coordination Chemistry*; Wilkinson, G., Gilard, R. D., McCleverty, J. A. Eds.; Pergamon: Oxford, England, 1987; Vol. 2, Chapter 20.

in the amino acid derivative or when the amino group is replaced by PPh_2. Furthermore, the deuterium isotopic effect and activation parameters for CO exchange observed herein for the tungsten complexes which exhibit this enhanced lability are compatible with such a reaction pathway. Attempts are currently underway to isolate π-stabilized unsaturated tungsten carbonyl complexes containing amido carboxylate ligands derived from pyrimidine derivatives. Indeed, recently we have synthesized and crystallographically characterized metal carbonyl derivatives of orotic acid, $[Et_4N]_2[M(CO)_4(orotate)]$ (M = Cr, W), and have shown that these complexes have very labile CO ligands as anticipated.[18,19]

Acknowledgment. Financial support of this research by the National Science Foundation (Grant CHE91-19737) and the Robert A. Welch Foundation is greatly appreciated.

Supporting Information Available: X-ray crystallographic files in CIF format for complexes **1**−**5** are available on the Internet only. Access information is given on any current masthead page.

IC961344M

(18) Draper, J. D.; Darensbourg, D. J. Presented at the 213th ACS National Meeting, San Francisco, CA, April 1997; Paper INOR 671.
(19) Darensbourg, D. J.; Draper, J. D.; Larkins, D. L.; Reibenspies, J. H. Unpublished observations.